Electronic Supplementary Material (ESI) for New Journal of Chemistry.

Supporting Information

A highly selective fluorescence sensor for Al^{3+} and CN^- in aqueous solution: biological applications and DFT calculations

Tae Geun Jo,[a] Jae Jun Lee,[a] Eunju Nam,[b] Kwon Hee Bok,[a] Mi Hee Lim,[b]* Cheal Kim*

[a]*Department of Fine Chemistry and Department of Interdisciplinary Bio IT Materials, Seoul National University of Science and Technology, Seoul 139-743, Republic of Korea. Fax: +82-2-973-9149; Tel: +82-2-970-6693; E-mail: chealkim@seoultech.ac.kr*

[b]*Department of Chemistry, Ulsan National Institute of Science and Technology (UNIST), Ulsan 44919, Republic of Korea. Fax: +82-52-217-5409; Tel: +82-52-217-5422; E-mail: mhlim@unist.ac.kr*

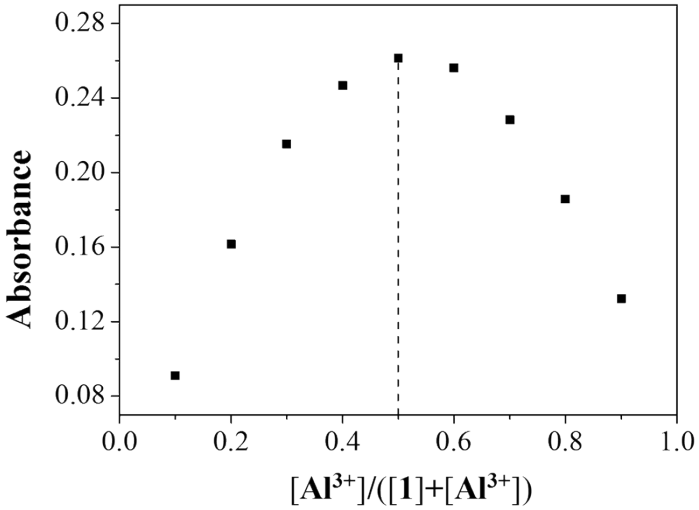

Fig. S1 Job plot for the binding of **1** with Al^{3+}. Absorbance at 310 nm was plotted as a function of the molar ratio $[Al^{3+}]/([\mathbf{1}] + [Al^{3+}])$. The total concentration of aluminium ions with receptor **1** was 1.0×10^{-4} M.

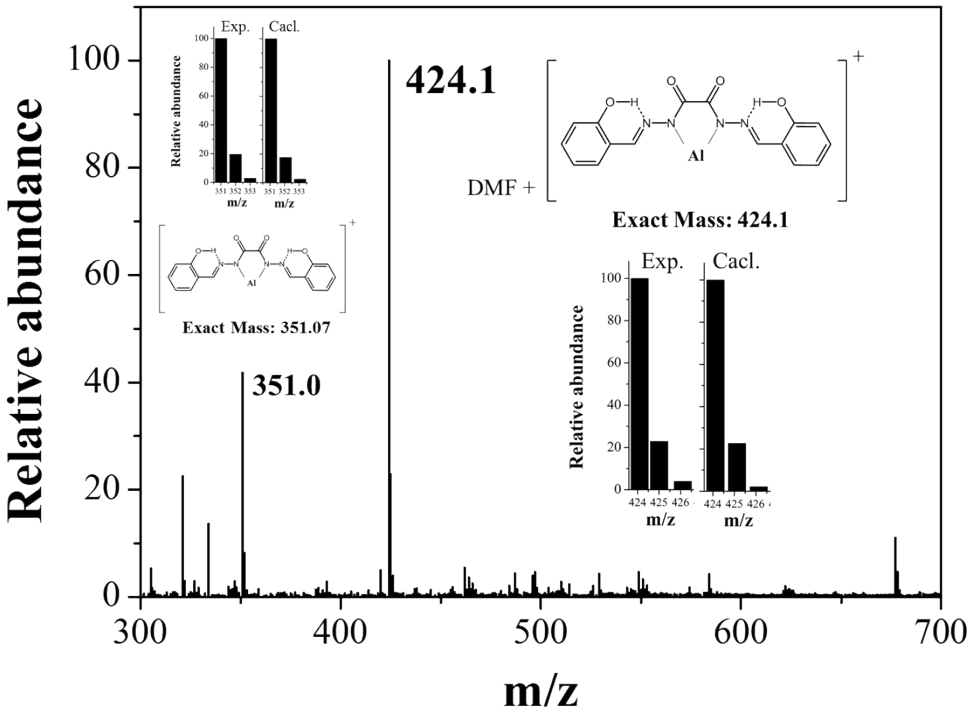

Fig. S2 Positive-ion electrospray ionization mass spectrum of **1** (10 μM) upon addition of $Al(NO_3)_3$ (1 equiv).

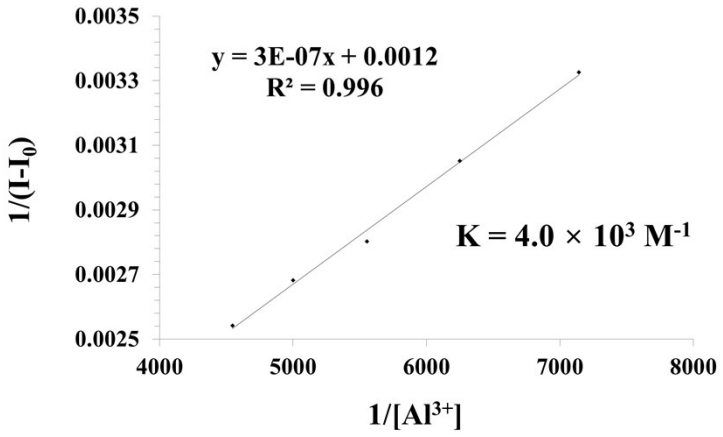

Fig. S3 Benesi-Hildebrand plot (fluorescence intensity at 491 nm) of **1** (5 μM), assuming 1:1 stoichiometry for association between **1** and Al^{3+}.

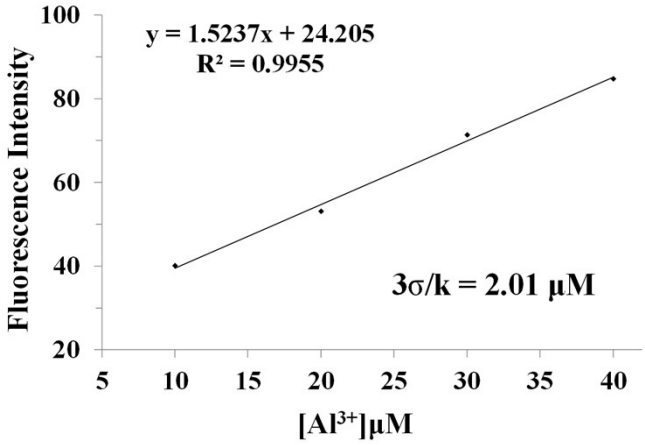

Fig. S4 Determination of the detection limit based on change in the ratio (fluorescence intensity at 491 nm) of **1** (5 µM) with Al^{3+}.

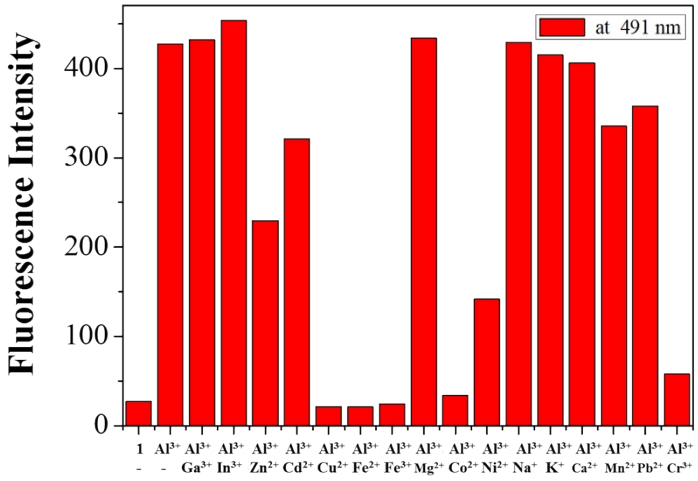

Fig. S5 Competitive selectivity of **1** (5 μM) toward Al^{3+} (52 equiv) in the presence of other metal ions (52 equiv) with an excitation of 410 nm in bis-tris buffer solution.

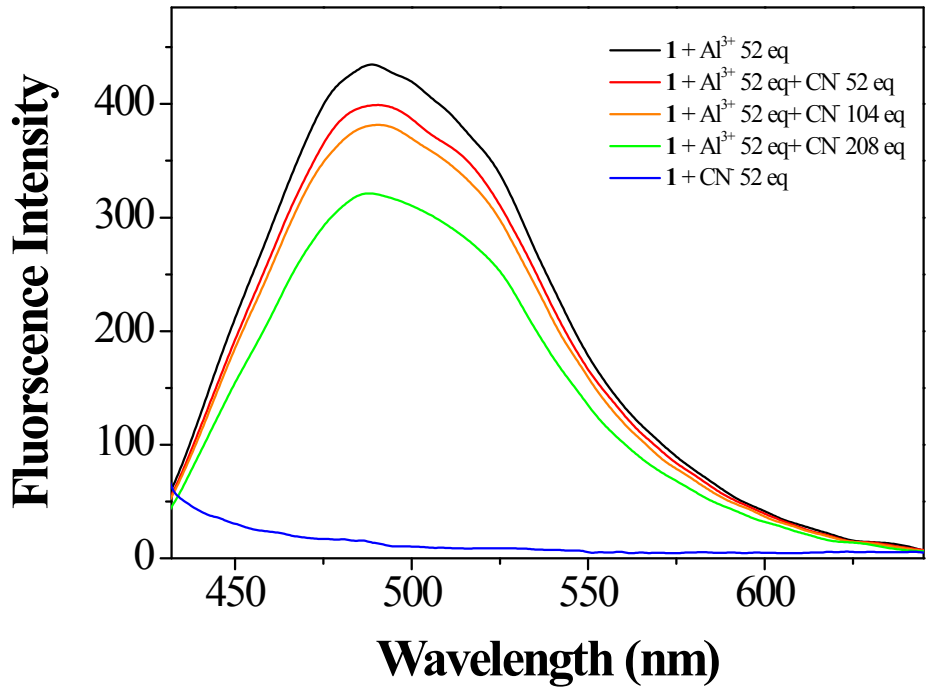

Fig. S6 Fluorescence spectral changes of **1** (5 μM) in the presence of Al^{3+}, CN^-, both Al^{3+} and CN^-, respectively, in bis-tris buffer solution.

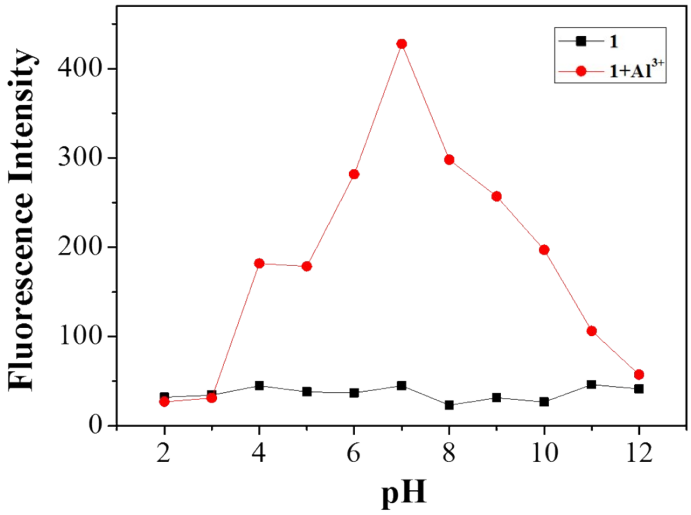

Fig. S7 Fluorescence intensity (at 491 nm) of **1**-Al^{3+} complex at different pH values (2-12) in bis-tris buffer solution.

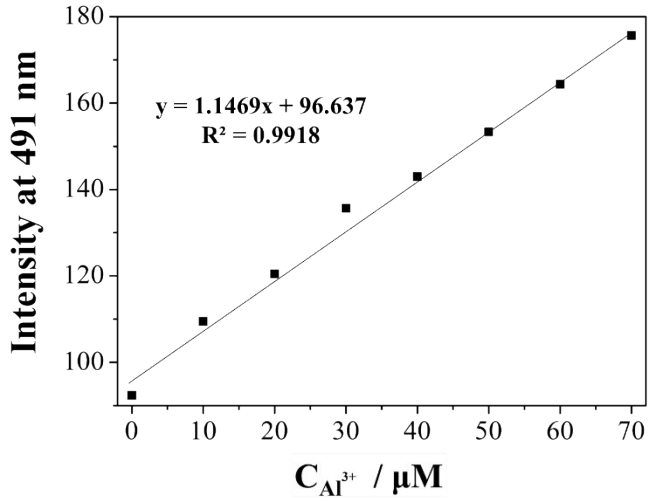

Fig. S8 Absorption (at 491 nm) of **1** as a function of Al^{3+} concentration. [**1**] = 15 μmol/L and [Al^{3+}] = 0-70.0 μmol/L.

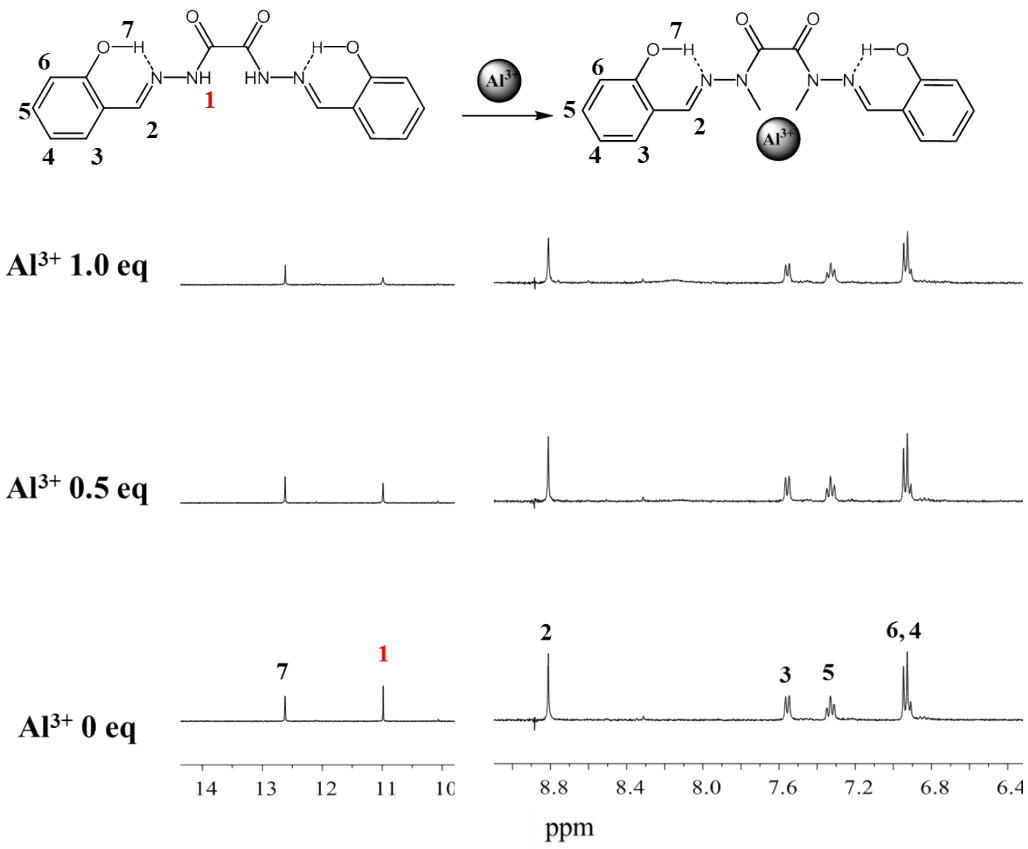

Fig. S9 ^{1}H NMR titration of receptor **1** with Al^{3+}.

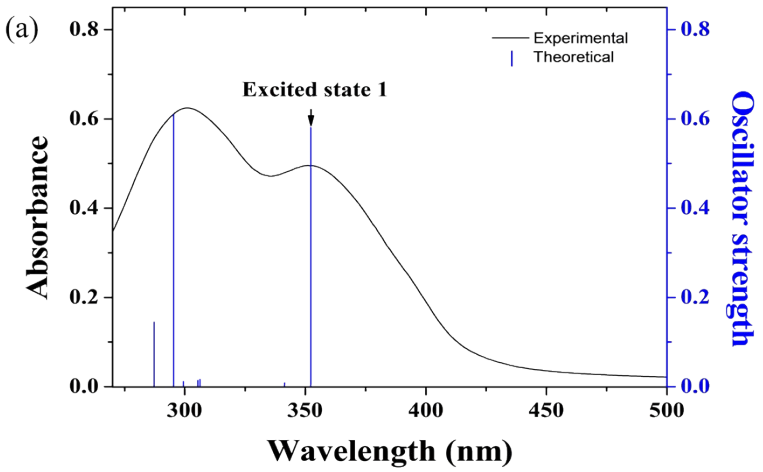

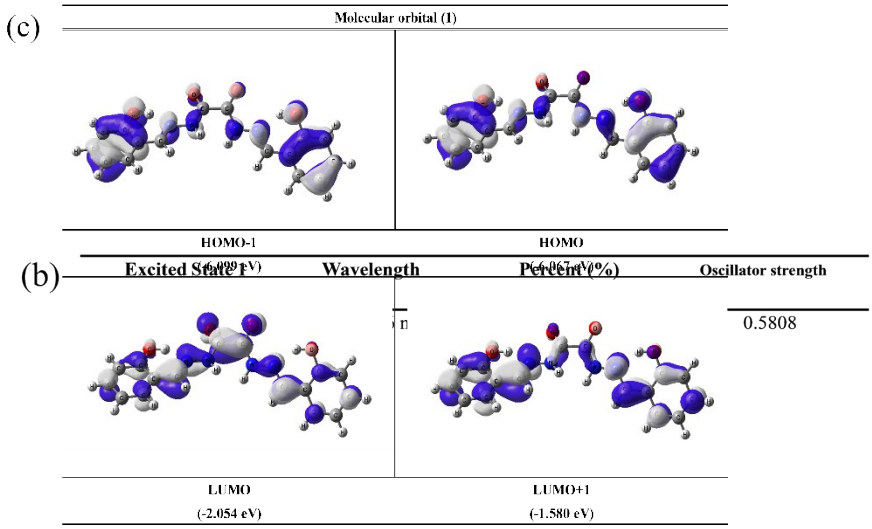

Fig. S10 (a) The theoretical excitation energies (TD-DFT method) and the experimental UV-vis spectrum of **1**. (b) The major electronic transition energies and molecular orbital

contributions for **1** (H = HOMO and L = LUMO). (c) Isosurface (0.030 electron bohr^{-3}) of molecular orbitals participating in the major singlet excited states of **1**.

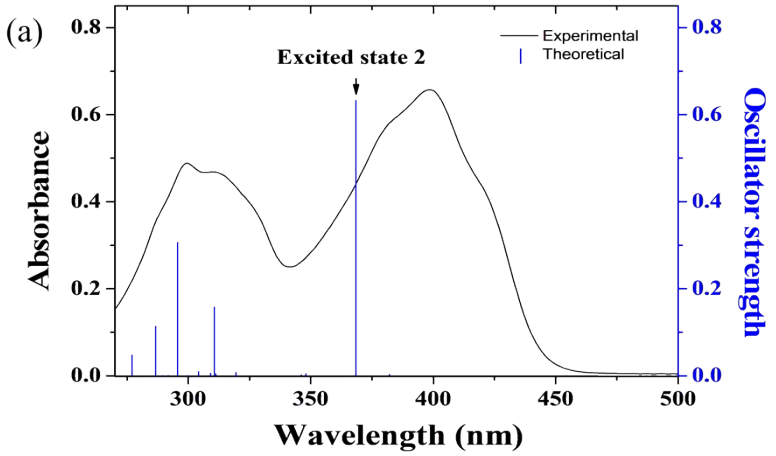

Fig. S11 (a) The theoretical excitation energies (TD-DFT method) and the experimental

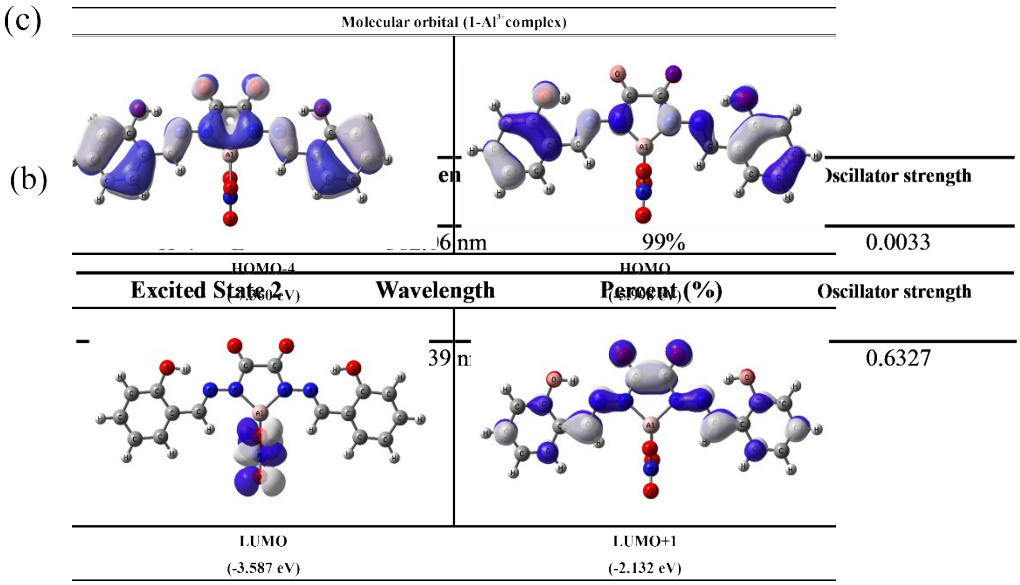

UV-vis spectrum of **1**-Al^{3+}. (b) The major electronic transition energies and molecular orbital contributions for **1**-Al^{3+} (H = HOMO and L = LUMO). (b) Isosurface (0.030 electron $bohr^{-3}$) of molecular orbitals participating in the major singlet excited states of **1**-Al^{3+}.

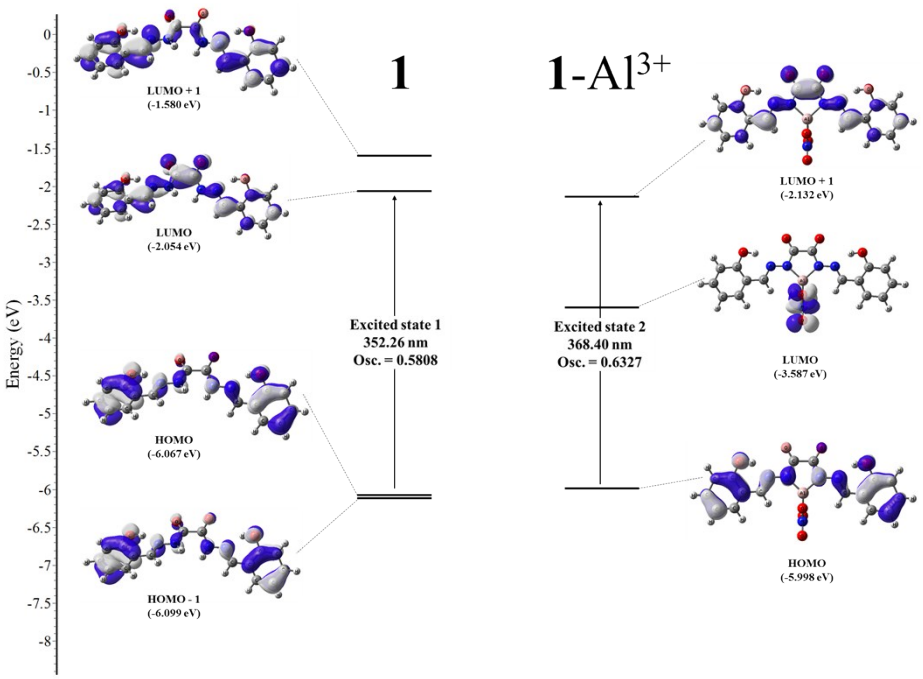

Fig. S12 Frontier molecular orbitals and their energies involved in the UV-vis absorption of **1** and **1**-Al^{3+} complex.

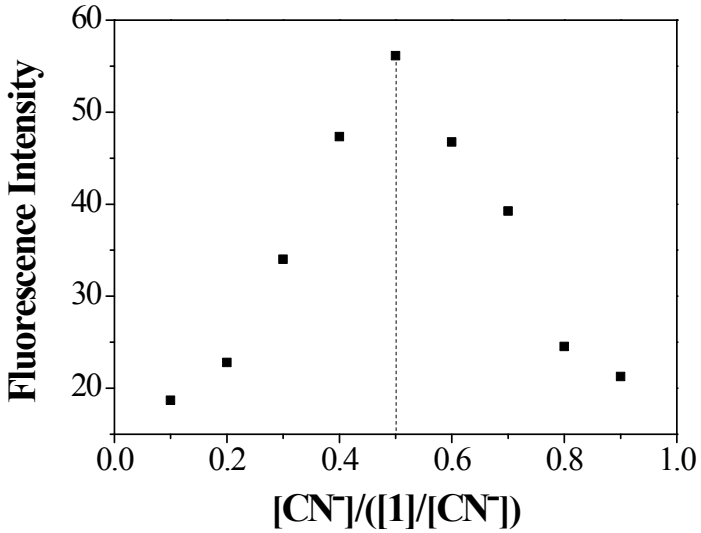

Fig. S13 Job plot for receptor **1** with CN^-. Fluorescence intensity at 522 nm was plotted as a function of the molar ratio $[CN^-]/([\mathbf{1}] + [CN^-])$. The total concentration of CN^- with receptor **1** was 1.0×10^{-4} M

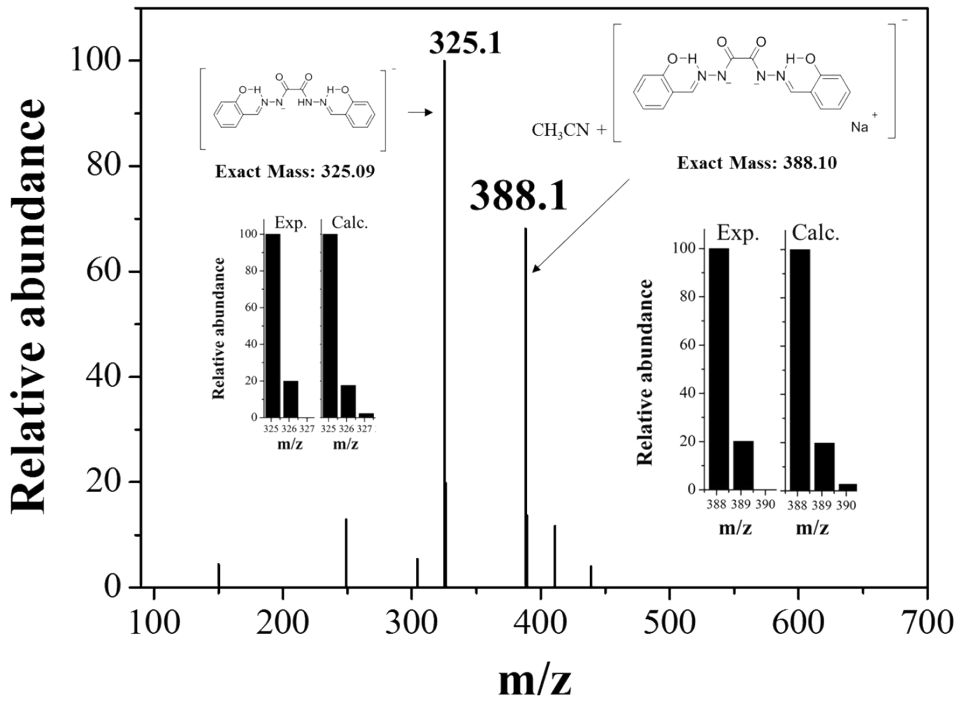

Fig. S14 Negative-ion electrospray ionization mass spectrum of **1** (10 μM) upon addition of TEA(CN) (5 equiv).

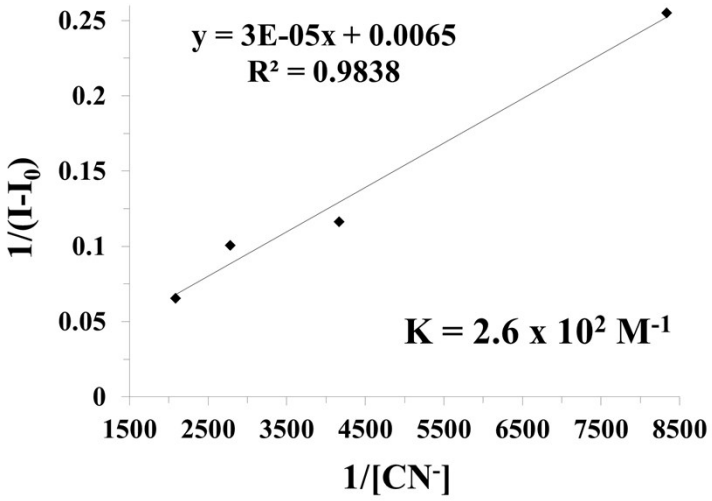

Fig. S15 Benesi-Hildebrand plot (fluorescence intensity at 522 nm) of **1** (30 μM), assuming 1:1 stoichiometry for association between **1** and CN^-.

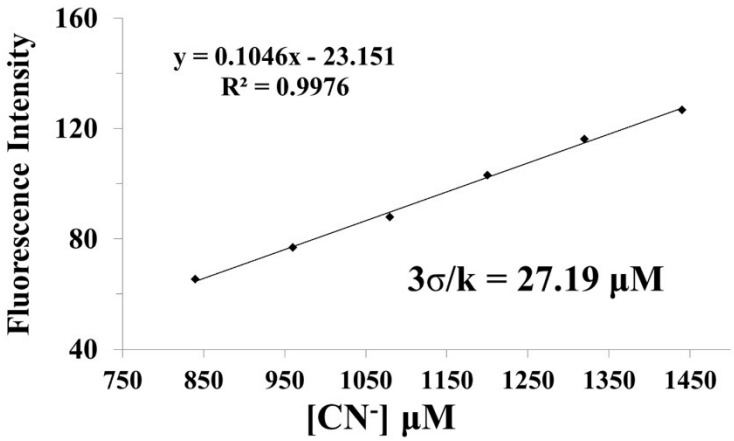

Fig. S16 Determination of the detection limit based on change in the ratio (fluorescence intensity at 522 nm) of **1** (30 µM) with CN^-.

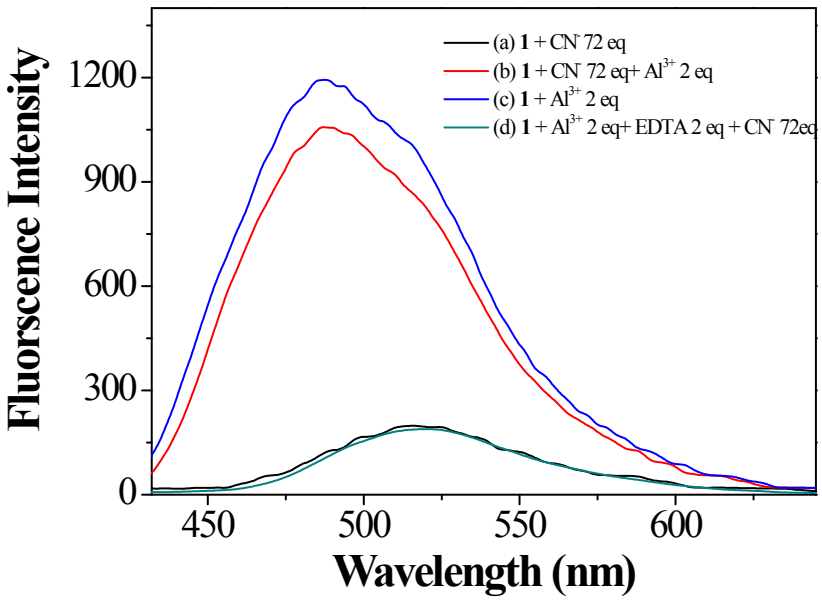

Fig. S17 Fluorescence spectral changes of **1** (30 μM) in buffer-DMSO (1:1, v/v) solution: (a) **1** + CN^- (72 equiv), (b) **1** + CN^- (72 equiv) + Al^{3+} (2 equiv), (c) **1** + Al^{3+} (2 equiv), and (d) **1** + Al^{3+} (2 equiv) + EDTA (2 equiv) + CN^- (72 equiv).

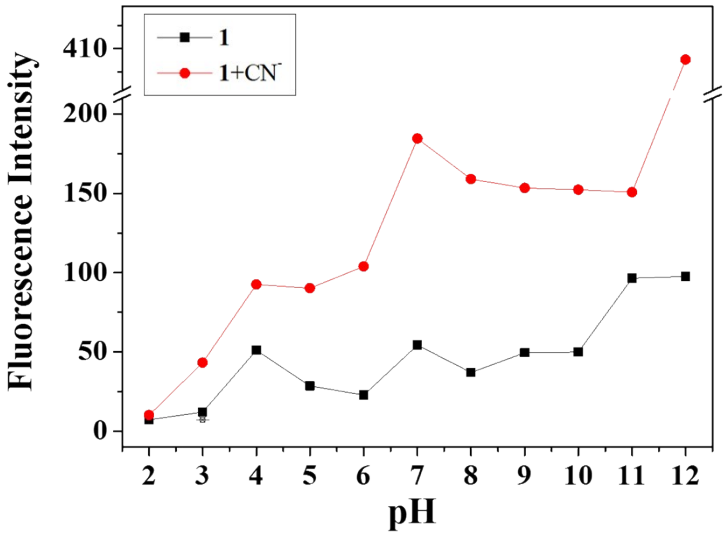

Fig. S18 Fluorescence intensity at 522 nm of **1** and **1**-CN species at different pH values (2-12) in bis-tris buffer solution.

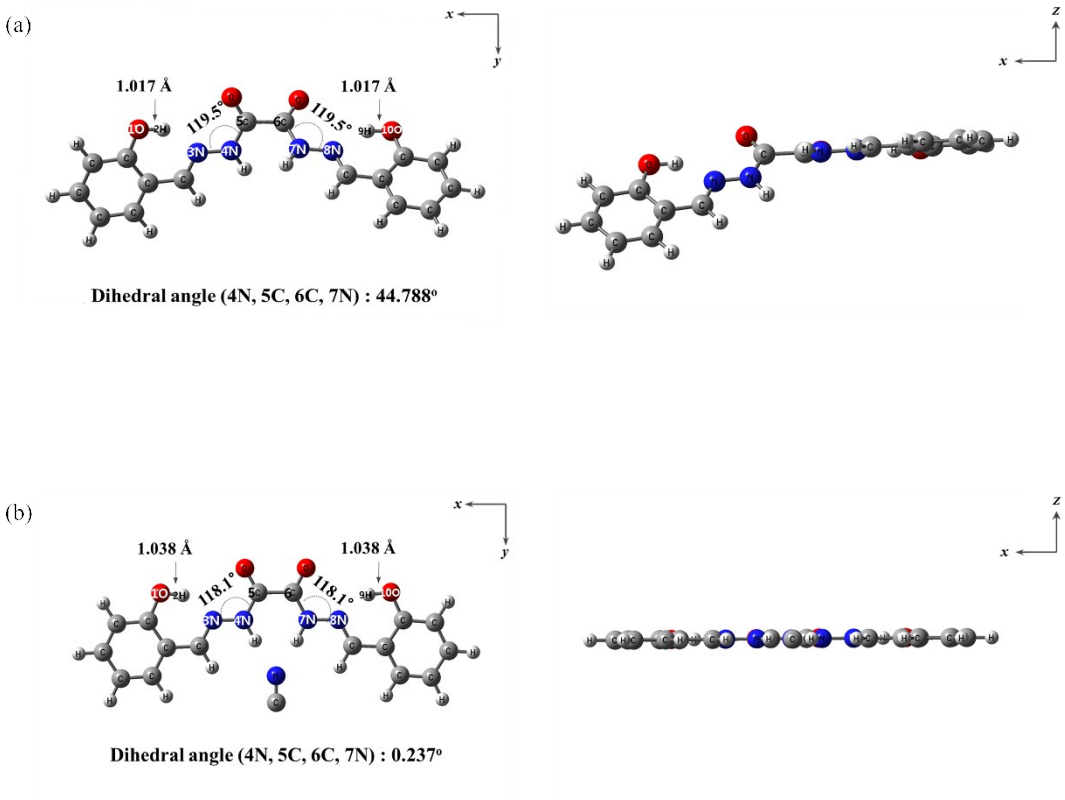

Fig. S19 Energy-minimized structures of (a) **1** and (b) **1**-CN^- from B3LYP level.

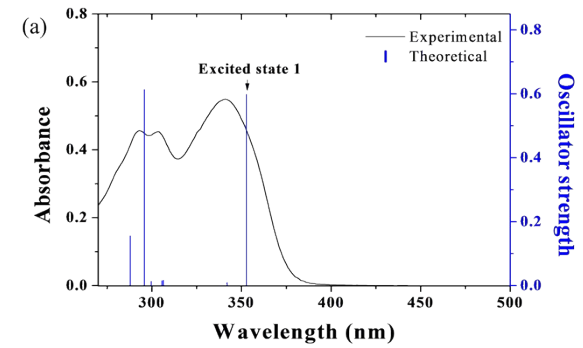

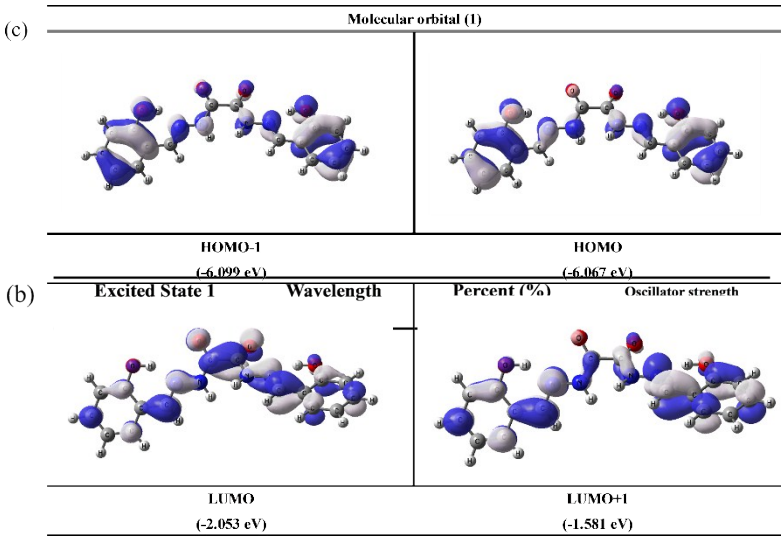

Fig. S20 (a) The theoretical excitation energies (TD-DFT method) and the experimental UV-vis spectrum of **1**. (b) The major electronic transition energies and molecular orbital contributions for **1** (H = HOMO and L = LUMO). (c) Isosurface (0.030 electron bohr^{-3})

of molecular orbitals participating in the major singlet excited states of **1**.

(a)

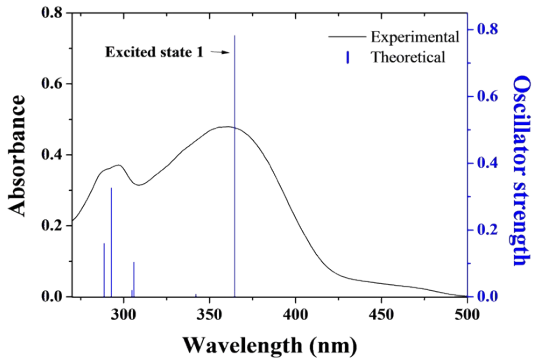

(b)

Excited State 1	Wavelength	Percent (%)	Oscillator strength
H → L	369.69 nm	98%	0.7824

(c)

Molecular orbital (1-CN$^-$)	
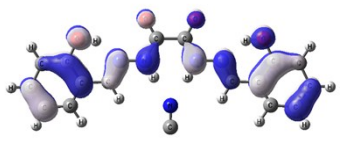	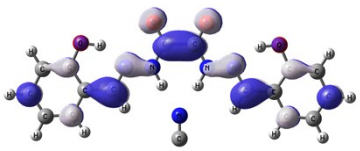
HOMO (-5.786 eV)	LUMO (-1.894 eV)

Fig. S21 (a) The theoretical excitation energies (TD-DFT method) and the experimental UV-vis spectrum of **1**-CN^-. (b) The major electronic transition energies and molecular orbital contributions for **1**-CN^- (H = HOMO and L = LUMO). (c) Isosurface (0.030 electron $bohr^{-3}$) of molecular orbitals participating in the major singlet excited states of **1**-CN^-.

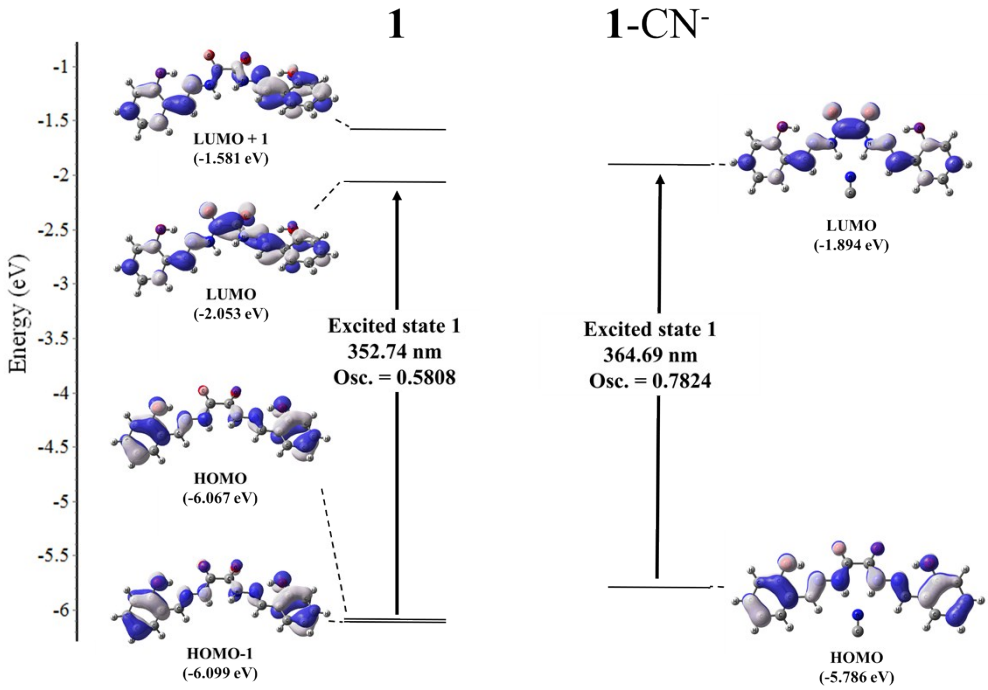

Fig. S22 Frontier molecular orbitals and their energies involved in the UV-vis absorption of **1** and **1**-CN^-